Sr-isotopic ratios trace mixing and dispersion in CO_2 push-pull injection experiments at the CO2CRC Otway Research Facility, Australia

Mike J. Bickle[1,*], Emily I. Stevenson[1], Ralf R. Haese[2,3]

[1] Dept. Earth Sciences, University of Cambridge, Downing Street, Cambridge CB2 3EQ

[2] Peter Cook Centre for CCS Research, School of Earth Sciences, The University of Melbourne, Parkville, VIC, 3010, Australia

[3] CO2CRC Ltd, 11-15 Argyle Place South, Carlton, VIC, 3053, Australia

* Corresponding author at: Department of Earth Sciences, University of Cambridge, Downing Street, CB2 3EQ, Cambridge, UK. *E-mail address:* mb72@esc.cam.ac.uk.

10/02/2020

Highlights:

$^{87}Sr/^{86}Sr$ ratios are consistent with conservative behaviour of Sr in push-pull injection experiments at the CO2CRC Otway CO_2 site

$^{87}Sr/^{86}Sr$ ratios and Sr concentrations allow calculation of fractions of 3 components in a subsequent injection experiment

Suggestions for improvements in experimental protocols for studying fluid mixing in heterogeneous reservoirs are presented

Keywords: Geological carbon storage; Push-pull injection; Sr-isotopes; CO2CRC Otway Research Facility; Hydrodynamic dispersion; Fluid tracers;

ABSTRACT

Analysis of $^{87}Sr/^{86}Sr$ ratios and modelling of formation water, injection water and produced water compositions from the CO2CRC Otway Research Facility in Victoria, Australia are used to test tracer behaviour and response in push-pull experiments. Such experiments are an essential pre-requisite to understanding the controls imposed by reservoir heterogeneities on CO_2 dissolution rates which may be an important stabilising mechanism for geological carbon storage. The experiments (Otway stage 2B extension in 2014) comprised two sequential tests in which ~ 100 tonnes of CO_2-saturated water was injected with combinations of Sr and Br or Li and Fluorescein tracers, each injection being followed by two staged extractions of ~ 10 tons and a final extraction of ~ 50 tons all spaced at ~ 10 day intervals. Analysis of the $^{87}Sr/^{86}Sr$ ratios of the produced fluids from the first injection, spiked with $SrCl_2$ and NaBr, is consistent with Sr behaving conservatively. This contrasts with previous interpretations in which Br was argued to have behaved conservatively while Sr, which dilutes ~ three times as fast as Br, was thought to be lost to a mineral phase. Such Sr-loss cannot explain the evolution of $^{87}Sr/^{86}Sr$ ratios. The analysis of $^{87}Sr/^{86}Sr$ ratios in the waters produced after the second injection episode, spiked with LiCl and Fluorescein tracers, allows calculation of the fractions of the formation waters and the injection waters from both tests 1 and 2. The Sr, Li and SO_4 tracers (the later formed by oxidation of formation sulphide) all indicate similar rates of dilution that is consistent with conservative behaviour. The results of the two injection episodes with spaced extractions are compared with two subsequent push-pull injections in which the produced waters, spiked with methanol, were extracted continuously. These continuous extraction experiments exhibited significantly less dilution over the same range of produced to injected water volumes (upto only ~ 0.6) than the earlier experiments with spaced extractions. This implies that some process related to the pauses in extraction enhances mixing of injected and formation waters. Achieving the objective of using push-pull experiments to assess reservoir heterogeneities and CO_2 dissolution rates will require better assessment of the various tracers to establish which behave conservatively followed a proper understanding of the causes of the variations in mixing as fluids are extracted from the formations.
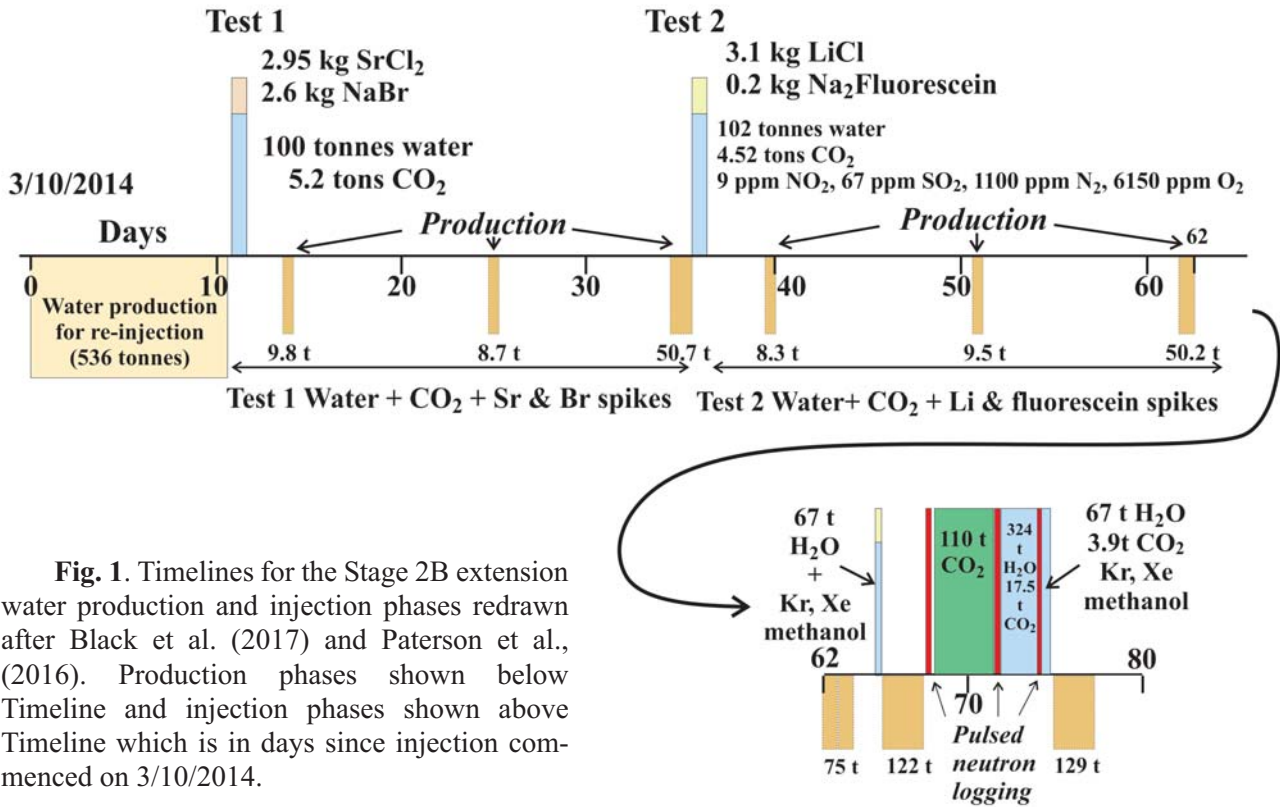
1   Introduction

Modelling the behaviour of soluble aqueous tracers is an essential part of field experiments to determine the aquifer properties which control the flow and mixing of fluids in the subsurface (e.g. Neuman, 1990). This is particularly applicable to the subsurface storage of carbon-dioxide which presents some of the most interesting challenges in interpretation of field experiments designed to measure the residual and dissolution trapping processes (e.g. Hovorka et al., 2006; Horvorka et al., 2011; La Force et al., 2014, Stalker et al., 2015). The problem is illustrated by the difficulties in reconciling differing estimates of residual trapping at the Otway site (e.g. Haese et al., 2013; La Force et al., 2014; Myers et al., 2015; Serno et al., 2016). These processes, the magnitude of which can only be confirmed by field trials, are likely to substantially increase the long-term security of CO_2 storage above that provided by impermeable caprocks (e.g. Kampman et al, 2016). The simplest field trials involve push-pull tests where water with tracers, CO_2 or CO_2-saturated waters are injected and then recovered with the objectives of estimating the impact of reservoir properties on mixing between injected and formation fluids, residual saturation of CO_2, dissolution of CO_2 and reactions between CO_2-charged fluids and formation minerals.

A series of push-pull experiments with injection of waters and CO_2 have been carried out at the CO2CRC Otway Research Facility in Victoria, Australia to monitor fluid mixing, fluid-mineral reactions and residual CO_2 saturation (Paterson et al. 2014; Haese et al., 2013; Dance and Paterson, 2016; Serno et al., 2016; Black et al., 2017; Ennis-King et al., 2017; Vu et al., 2017; Vu et al., 2018). Here we present analyses of $^{87}Sr/^{86}Sr$ ratios in fluids sampled from two push-pull experiments that injected CO_2-saturated waters mixed with various soluble tracers. The results suggest a re-evaluation of the previous interpretations of the relative behaviours of the Sr, Br and Li tracers, confirm the utility of measurements of isotope ratios in addition to concentrations as tests of mass balance calculations and raise important questions about the nature of mixing in the formation. Understanding mixing and dispersion in heterogeneous formations is critical to using partitioning tracers to measure residual CO_2 saturations (e.g. LaForce et al., 2014) and will be critical to field experiments designed to measure dissolution trapping (e.g. Benson et al., 2018).

2   The Otway 2B Experiments

The Otway 2B experiments injected and produced fluids from a 7m perforated interval between 1392 and 1399 m TVDSS in the Otway well CRC-2 (Temperature ~ 60° C, pressure ~ 14 MPa) (Paterson et al., 2014). The interval is near the top of Parasequence 2 in the Paaratte Formation Unit A and comprises coarse deltaic sandstones with an average porosity of 28% and horizontal permeability of $2.3x10^{-12}$ m^2 (2.3 darcy). The 7 m interval is bounded above and below by essentially impermeable carbonate-cemented sandstones (Dance and Paterson, 2016). The experiments took place in two stages in 2011 and 2014. In 2011 (Stage 2B), using produced water from the formation, a series of water injections (~ 100 t), CO_2 injection (250 t), CO_2-saturated water injection (~450 t, then ~100 t), interspersed with water production phases were designed to estimate residual CO_2 saturations by neutron residual saturation measurements, thermal perturbations and partitioning tracer tests (Paterson et al., 2014). In 2014 Stage 2B extension, again using produced water, initiated with two injection (~100 t each) and withdrawal phases (~70 t each) injecting formation waters spiked with SrCl and NaBr (Test 1) and LiCl and Fluorescein (Test 2) (Fig. 1, see also Fig. 12). These 'Tests' were followed by injection of 67 t of water spiked with methanol, Kr and Xe, production of 122 t of water, followed by injection of 110 t of CO_2 which was then driven to residual saturation by injection of 324 t of CO_2-saturated water followed by injection of ~67 t of CO_2-saturated water spiked with methanol, Kr and Xe and then production of ~130 t of water (Ennis-King et al., 2017; Paterson et al. 2016; Serno et al., 2016) (Fig. 1). Test 1 and Test 2 each had three phases of water production with time gaps of ~10 days between extraction phase 1 and 2 and 2 and 3 to allow for reactions between the CO_2 saturated waters and reservoir

Fig. 1. Timelines for the Stage 2B extension water production and injection phases redrawn after Black et al. (2017) and Paterson et al., (2016). Production phases shown below Timeline and injection phases shown above Timeline which is in days since injection commenced on 3/10/2014.

minerals. This contrasts with subsequent injection of water spiked with methanol, Kr and Xe which were produced continuously.

In this study the $^{87}Sr/^{86}Sr$ ratios of formation waters, injection waters and produced waters from Tests 1 and 2 have been analysed and used to test models of Sr-mixing between injected waters and formation waters in comparison with the other tracers. The $^{87}Sr/^{86}Sr$ ratios, which are not fractionated by fluid-mineral reactions and analysed to high precision, provide stringent tests of fluid mixing models. The Test 1 and 2 experiments, with periodic extraction, exhibit very different mixing relationships to the results of the later methanol, Kr and Xe spiked injections which were produced continuously.

3   Analytical Methods

The water samples were aliquots of samples previously analysed by Black et al. (2017) (Table S1, supplementary information), cations by inductively coupled plasma-atomic emission spectroscopy and anions by ion chromatography. Averages of the duplicate samples taken by U-tube are used and the precisions of the concentration analyses (σ_i for element i) given in Table S1 are estimated from the root mean square of the standard deviations of the duplicates. That is

$$\sigma_i = \sqrt{\frac{\sum_{j=1}^{n} \sigma_j^2}{n}} \tag{1}$$

where σ_j is the standard deviation of each of the n duplicates (n=19 in both Tests 1 and 2). The precisions of the analyses of the formation waters sampled before Test 1 and the Test 1 injection waters are taken as the standard error of the 3 formation water samples and 4 injection water samples where these are greater than the precisions based on the duplicates of produced waters.

Sr was separated using Eichrom Strontium specific resin and the $^{87}Sr/^{86}Sr$ ratio analyses made on a Thermo Scientific Triton Plus multicollector solid-source mass-spectrometer. Analyses were performed in static mode using Faraday cups. $^{87}Sr/^{86}Sr$ ratios were corrected using an exponential fraction

correction to an $^{86}Sr/^{88}Sr$ ratio = 0.1194. External accuracy is indicated by analysis of 7 repeats of the NBS987 standard which gave 0.710257 ± 5 (1σ). Sr blanks during the chemical processing (always < 700 pg) are small compared to the sample size analysed (250 ng).
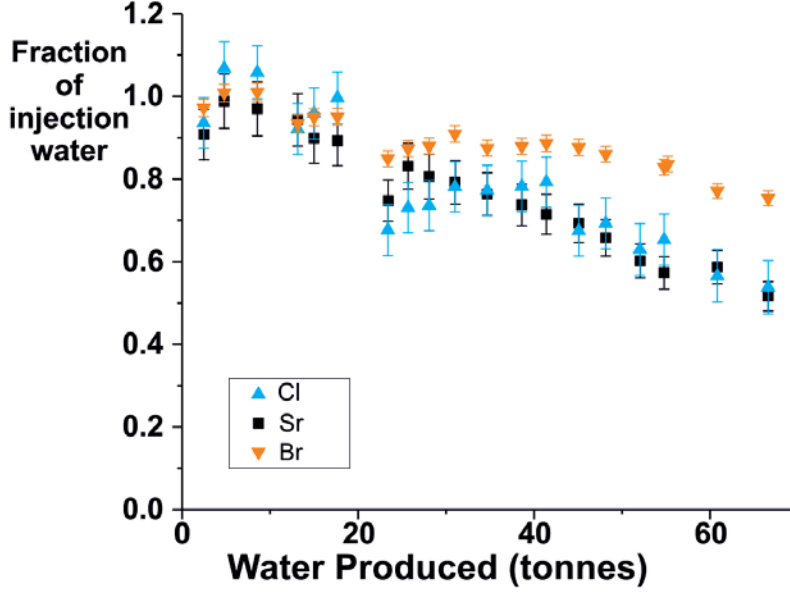
4   Test 1

Figure 2 illustrates the evolution of Sr and Br concentrations as a function of the volume of water produced after the Test 1 injection. SrCl and NaBr were introduced as spikes in Test 1 and both are progressively diluted with increasing produced water. Both tracers exhibit unsteady behaviour against the volume of produced water. The initial samples from extraction phases 1 and 3 exhibit markedly low Sr concentrations. The initial two samples of extraction phases 1 and 2 and the initial 3 samples of extraction phase 3 exhibit low and increasing Br concentrations. This may reflect extraction of water from a high permeability damage zone adjacent to the injection well in which excess mixing took place during the pauses between production phases (c.f. Haese et al., 2016). It should be noted that the injection of 100 t of water into a 7 m interval in a formation with a porosity of 0.28 would only extend ~ 4 m on average and a 15 cm radius damage zone, porosity ~ 0.3, plus the fluid within the 5½" casing would contain ~ 0.4 tonnes of water. The contrast between the behaviour of Br and Sr is intriguing given the discussion below. However after the initial increases in concentration in each pumping phase both Br and Sr exhibit near-linear decreases with the volume of produced water.

A further complication is that during the Otway 2B project in 2011 ~ 150 t of CO_2 and ~ 560 t of CO_2-saturated formation water were injected (with ~ 350 t produced) in the same borehole interval and the CO_2-rich formation waters reacted with reservoir minerals over the intervening three years. For example Ca increased from ~ 95 μmol/L in formation water prior to the 2B project to ~ 1400 μmol/L in produced water at the end of the project (Kirste et al., 2014). Three years later in 2014 Ca had then increased to ~3600 μmol/L at the start of water production for the 2B extension experiment then decreased to 3000 μmol/L after the initial production of 500 t of water (Haese et al., 2016). The other elements (Mg, Na, Si, Sr) showed similar decreases during the 500 t of initial water production for the 2B extension experiment although Cl increased from ~ 4400 to 5200 μmol/L. It is possible that injected waters mixed with formation waters more dilute than the samples collected by U-tube immedi-
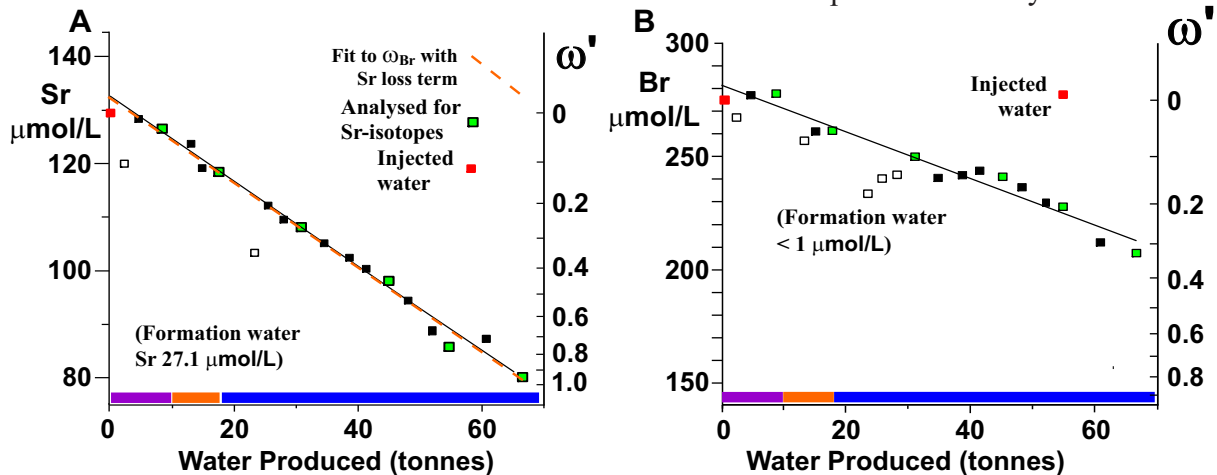
Fig. 2. Variation of Sr and Br concentrations in U-tube waters sampled during the 3 production phases in Test 1 plotted against volume of produced water. Coloured bar shows three pumping episodes starting ~ 3, 14 and 24 days after injection. Samples shown by green symbols are those analysed for Sr-isotopic ratios. Right hand axes show ω', the fraction of formation water added to cause the observed decrease in Sr or Br calculated from equation 2. The lines are least-squares linear fits with samples shown by open symbols excluded from the fits for Sr as these two samples are much lower than the subsequent samples (see text). The fit to the Sr data using the fraction of formation water added, ω', calculated from the Br data and with a Sr-loss term (dashed line in A) is indistinguishable from the linear fit. Statistical information on the linear fits is given in Table S2 in Supplementary Information.

Fig. 3. Fraction of injection water, $(1/(1+\omega)$ where ω is defined in equation 2) as a function of volume of produced water in Test 1, calculated from Sr, Br and Cl concentrations assuming conservative behaviour. 1σ uncertainties of 1.1% for Sr, 0.9% for Br and 0.5% for Cl are calculated from duplicates of the produced water samples. Uncertainties on injection and formation water analyses calculated from standard error on 3 repeat analyses of formation waters and four repeats of injection waters where these are larger than fractional errors calculated from duplicated samples.

ately prior to the Test 1 injection. However Sr and Br are sufficiently dilute prior to Test 1 that mixing with even more dilute pristine formation water would make a negligible difference to the sampled fluids. The non-systematic variations of Sr, Br and Cl with mass of produced water (Figs. 2 & 3) are likely to reflect variations in the amount of formation water mixed with injected water.

Cl also exhibits dilution during water production although the relative high Cl in the formation water (5114 μmole/L) compared to the injection water (5613 μmole/L) makes the estimates less precise and more sensitive to potential changes in formation water composition but the precision of the Cl analyses (0.5% 1σ) is sufficient to make the calculations meaningful. Fig. 3 compares the dilution of Sr, Br and Cl with errors based on the precision of the duplicate analyses.

Sr and Cl decrease faster than Br. The relative mass of formation water, ω', added to unit mass of injection water, assuming conservative mixing, may be calculated as

$$\omega' = \frac{C_{inj} - C_p}{C_p - C_f} \qquad 2$$

where, C_{inj} is the concentration of the tracer in the injected water, C_p the concentration in the produced water and C_f, the concentration in the formation water. The calculated ratio of formation water to injection water by the end of production is ~ 1 for Sr but only 0.3 for Br. As Black et al., (2017) discuss, this may be because Sr is not conservative and is lost to a solid phase in the reservoir or during production. However the variation in Sr-isotopic compositions during production (Fig. 4A) matches conservative behaviour within the uncertainty of the analyses where the ^{87}Sr/^{86}Sr ratio of the sampled water ($^{87}Sr_p$) is calculated from the Sr concentration as

$$^{87}Sr_p = \frac{\left(^{87}Sr_{inj}.Sr_{inj} + \omega_{Sr}.^{87}Sr_f.Sr_f\right)}{\left(Sr_{inj} + \omega_{Sr}.Sr_f\right)}. \qquad 3$$

where Sr_{inj} and $^{87}Sr_{inj}$ are the Sr concentration and ^{87}Sr/^{86}Sr ratio of the injected water (129.5 μmol/L and 0.707486), Sr_f and $^{87}Sr_f$ are the Sr concentration and ^{87}Sr/^{86}Sr ratio of the formation water (27.1 μmol/L and 0.707006), and ω_{Sr} is calculated from equation 2. The errors are calculated by a Monte Carlo routine randomly varying all the parameters in equations 2 and 3 with 1σ Gaussian uncertainties
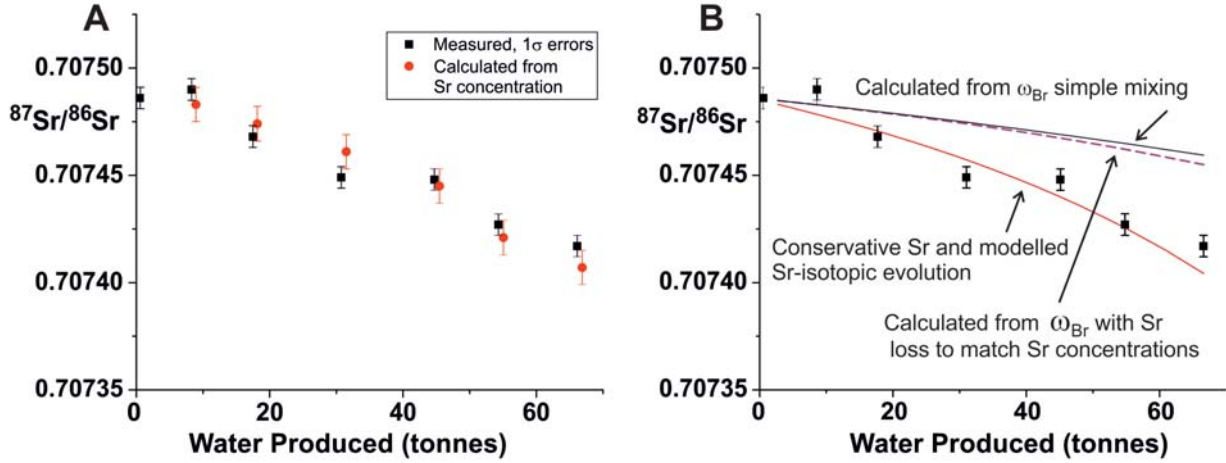
Fig. 4A. Comparison of measured ^{87}Sr/^{86}Sr ratios (black squares) in samples from Test 1 with ^{87}Sr/^{86}Sr ratios calculated from fraction of formation water calculated from Sr concentrations (ω_{Sr}, equation1) mixed with injection water (Concentrations given in Table S1). 1σ error bars on measured samples are external errors on duplicate samples. 1σ error bars on calculated values are from a Monte Carlo routine assuming 1.1% (1σ) uncertainty on concentrations and 5x10^{-6} (1σ) on ^{87}Sr/^{86}Sr ratios. Fig. 4B compares measured ^{87}Sr/^{86}Sr ratios (black squares) with 1) evolution of ^{87}Sr/^{86}Sr ratios (black solid line) calculated assuming Sr behaves conservatively and dilution of injection water is calculated from linear fit to Br concentration data (Fig. 2B), 2) evolution of ^{87}Sr/^{86}Sr ratios (purple broken line) given dilution of injection water from Br with a Sr-loss term to match Sr concentrations (equation 6) and, 3) evolution of ^{87}Sr/^{86}Sr ratios (red solid line) calculated assuming Sr behaves conservatively as linear fit to Sr concentration data (Fig. 2A).

on the Sr concentrations of the produced water of 1.17%, on the injected water of 6.7% and on the formation water of 8% and on ^{87}Sr/^{86}Sr ratios of 5x10^{-6}.

Since the Br data imply less dilution of the injected waters as a function of the volume of produced water, mixing of the formation waters with the injected fluid volumes calculated from the dilution of Br results in a slower decrease in Sr-isotopic ratios than the measured values (black curve on Fig, 4B). If Sr has been lost by precipitation of, or exchange with, a mineral phase in the reservoir the ^{87}Sr/^{86}Sr ratio of the produced fluids would be expected to decrease more rapidly with the volume of produced water as injected Sr is taken out of solution. This may be modelled by fitting an expression for the variation in Sr in the produced fluids that assumes dilution factors calculated from the decrease in Br and includes a term for Sr loss as a function of the volume of produced water to match the variation in Sr. To do this the concentration of Sr (Sr_p) is modelled as varying with the fraction of formation water added, calculated from the dilution of Br (ω_{Br}),

$$Sr_p = \frac{Sr_{inj} + \omega_{Br}\left(Sr_f - L\right)}{\left(1 + \omega_{Br}\right)} \qquad\qquad 4$$

and ω_{Br} is related to the volume of water produced by the least-squares linear best-fit to the variation of Br in the produced water (Br_p) in Fig. 2B

$$Br_p = A + B.V \qquad\qquad 5$$

where $A = 281.0 \pm 2.7$ µmol/L, $B = -1.03 \pm 0.06$ µmol.L^{-1}.t^{-1}. Fitting equation 4 to the variation of C_{Sr} against ω_{Br}, where ω_{Br} is calculated from fit described by equation 5 with Sr_{inj} and (Sr_f -L) as unknowns, gives a value for L of 110.1 ± 5.1 and $Sr_{inj} = 132.3 \pm 0.9$ µmol/L, the later close to the measured value of 129.5 ± 6.7 (1σ) µmol/L. This best-fit is indistinguishable from the linear fit to the Sr data (Fig. 2A). The calculation of the Sr-loss term, L, from ω_{Br} derived from the best-fit relationships between Br and the volume of produced fluid provides a convenient method for averaging the data. Cal-

culating *L* for samples sufficiently evolved to have 1σ uncertainties <60%, (that is sample 2BX-W-L262 and later samples) from equation 4 with ω_{Br} given by equation 2 gives a similar mean value (128 ± 40 μmol/L, 1σ) but the uncertainties on the individual samples are of order 50% or more.

The predicted variation of Sr-isotopic compositions may then be calculated from mass balance as

$$\frac{\partial\left(^{87}Sr_p \, Sr_p \, (1+\omega_{Br})\right)}{\partial\omega_{Br}} = {}^{87}Sr_f . Sr_f - L . {}^{87}Sr_p \qquad 6$$

with the concentration of Sr in the formation water, Sr_p, varying as equation 3. The solution of equation 5 is

$$^{87}Sr_p = {}^{87}Sr_f + \left(^{87}Sr_{inj} - {}^{87}Sr_f\right) . \frac{\left(Sr_{inj} + \left(Sr_f - L\right)\omega_{Br}\right)^{-Sr_f/(Sr_f - L)}}{Sr_{inj}^{-Sr_f/(Sr_f - L)}} . \qquad 7$$

The predicted $^{87}Sr/^{86}Sr$ ratios of the produced waters decrease more rapidly than with simple dilution (compare red dashed and solid black curves on fig. 4B) but the difference is small and the values lie well outside the 2σ uncertainty estimates of the measured $^{87}Sr/^{86}Sr$ ratios. If the dilution of the injected waters calculated from the Br data is correct then the Sr-isotopic compositions must be buffered by Sr exchange with minerals in the reservoir of exactly the correct magnitude and Sr-isotopic composition to simulate conservative mixing. This seems unlikely although why Br concentrations should decrease less than predicted from the Sr data has not been explained.
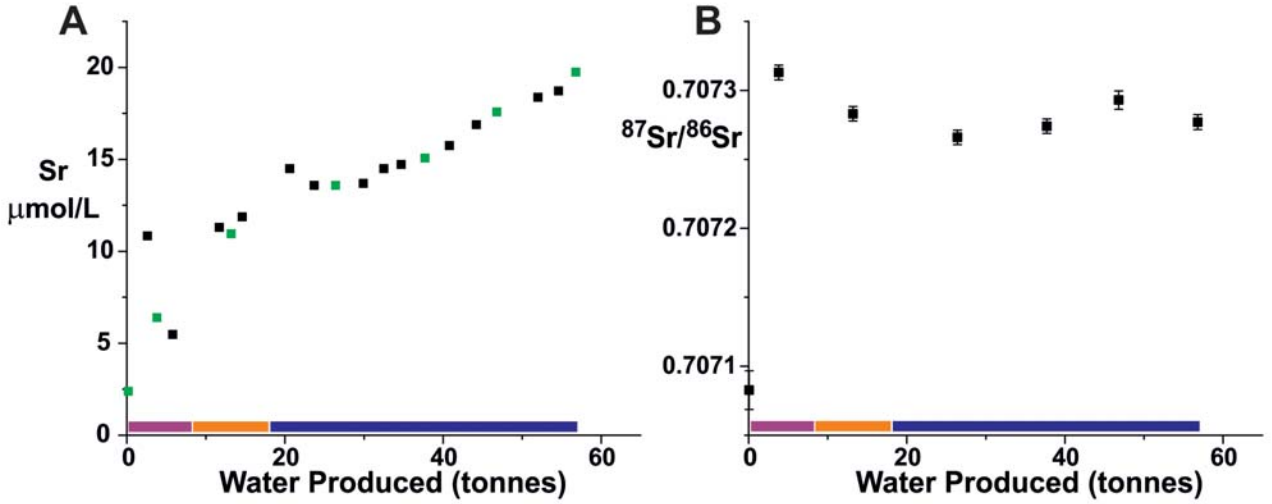
5   Test 2

The Test 2 CO_2 saturated injection waters were spiked with LiCl and Na_2Flourescein with the gasses NO_2, SO_2, N_2 and O_2 added to the CO_2. Figure 5 illustrates the fraction of injection water in the produced water from the variations of Li, Cl, Flourescein and SO_4 where the ratio of formation water added (ω) is calculated from equation 2, given that the concentrations of all the spikes in the formation waters are small. As discussed by Black et al., (2017), flourescein is probably lost to mineral surfaces in acidic waters. SO_4 is formed by oxidation of sulphide minerals and the injection water composition after reaction (48 ppm) was estimated by Black et al., (2017) by comparison with the Li data. Li, Cl and SO_4 dilute to ~ 50% comparable to Sr in Test 1 for similar volumes of injected and produced wa-
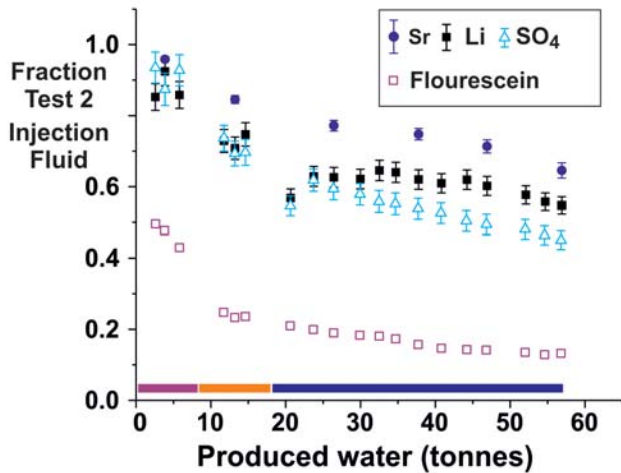
Fig. 5. Fractions of Test 2 injection fluid ($1/(1+\omega')$) calculated from equation 2 assuming formation waters have the same composition prior to Test 1, plotted against volume of produced water for Li, SO_4, Cl and Flourescein. 1σ error bars reflect precisions of 3.1% for Li and 2.4% for SO_4 calculated from duplicate analyses. Calculation for Sr is based on deconvolution of Sr concentrations and $^{87}Sr/^{86}Sr$ ratios (equations 8 & 9 - see text). As discussed by Black et al., (2017), Flourescein is probably lost to mineral surfaces in acidic waters. SO_4 is formed by oxidation of sulphide minerals and the injection water composition after reaction (48 ppm) was estimated by Black et al., (2017) to give the best fit to the Li dilution data for the initial sample. Coloured bar shows the three phases of water production.

Fig. 6. Sr and [87]Sr/[86]Sr variation with volume of produced water in Test 2. Green symbols in Fig. 6A are samples analysed for Sr-isotopic composition. Note that the low [87]Sr/[86]Sr ratio of the injection water has limited impact on the [87]Sr/[86]Sr ratio of the produced waters which show increasing Sr concentrations as injected water is diluted by formation water mixed with injection waters from Test 1. Coloured bar shows the three water production phases. Error bars in Fig. 6B are 1σ.

ters. Interestingly Li, Cl, flourescein and SO_4 all show similar trends with more rapid dilution in the first two phases of production followed by a shallower linear dilution trend in phase 3. The first samples of Li, Cl and SO_4 in phase 3 exhibit low Li and SO_4 concentrations in a similar manner to the test 1 tracers.

Sr was not injected as a tracer in Test 2. The Test 2 injection waters contained very low Sr (~2.4 μmol/L). The Sr concentrations rise monotonically but [87]Sr/[86]Sr ratios vary in a more complex manner (Fig. 6) reflecting the three sources of Sr, formation waters, Test 1 injection waters and Test 2 injection waters.

Since the Test 1 and Test 2 injection waters and the formation water have different Sr concentrations and Sr-isotopic ratios (Fig. 7A) the respective Sr and Sr-isotopic mass-balance equations

$$Sr_p = A.Sr_{inj-1} + B.Sr_{inj-2} + C.Sr_f \qquad\qquad 8$$

$$^{87}Sr_p = \frac{A.Sr_{inj-1}.^{87}Sr_{inj-1} + B.Sr_{inj-2}.^{87}Sr_{inj-2} + C.Sr_f.^{87}Sr_f}{A.Sr_{inj-1} + B.Sr_{inj-2} + C.Sr_f} \qquad\qquad 9$$

may be solved for the fractions of each input. A is the fraction of Test 1 injection water, B is the fraction of Test 2 injection water, C is the fraction of formation water ($A + B + C$=1). Sr_{inj-1}, $^{87}Sr_{inj-1}$, Sr_{inj-2}, $^{87}Sr_{inj-2}$, Sr_f, $^{87}Sr_f$, and Sr_p and $^{87}Sr_p$ are the Sr concentrations and isotopic ratios of the Test 1 injection waters, Test 2 injection waters formation water and the sampled produced water.

The results (Fig. 7B) indicate that the ratio of Test 1 injected water to formation water is ~ 2 in the first sample, similar to the final samples from Test 1 but that this ratio decreases rapidly. The fraction of Test 2 injection water decreases monotonically with the volume of produced water at rate that mirrors the dilution of Cl and at a slightly lower rate than implied by Li and SO_4. The final dilution calculated from the Sr data is 65% which compares to 55% for Li and 45% for SO_4. Given the 2σ propagated uncertainties of about 5% (absolute) these values are not far outside error. This is illustrated in Fig. 8 in which the measured Br, Li and Cl concentrations are compared with those calculated from the proportions of Test 1 injection, Test 2 injection and formation waters given by the Sr systematics and the injection and formation water compositions.
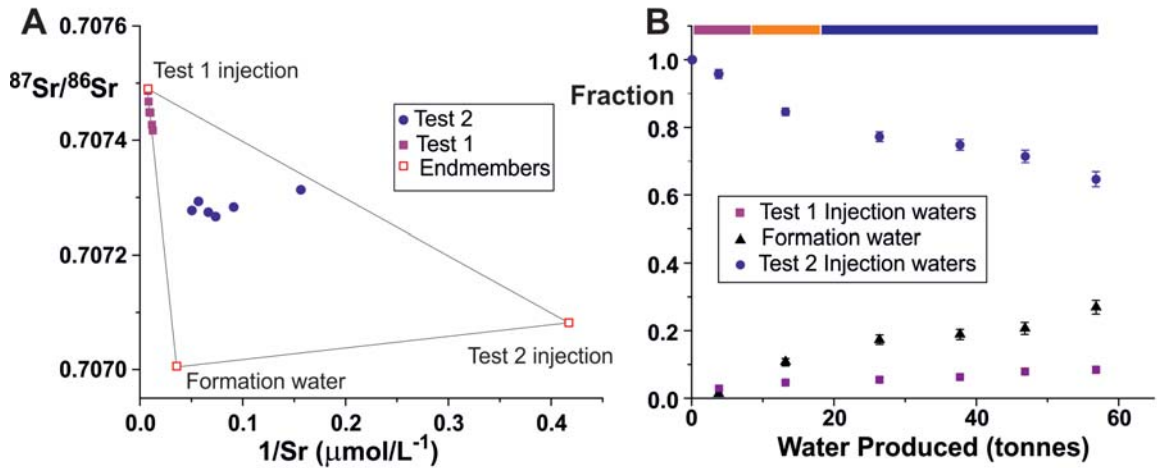
Fig. 7A. $^{87}Sr/^{86}Sr$ ratios plotted against 1/Sr illustrating two component mixing in Test 1 and 3 component mixing in Test 2. **Fig. 7B** shows fractions of Test 1 injection water, Test 2 injection water and formation water calculated from mass balance (equations 7 and 8) with 1σ uncertainties estimated by a Monte Carlo routine with the same uncertainties on the Sr data as used for Fig. 4. Error bars are not shown where smaller than symbols. Coloured bar delineates the three production phases.

The Br concentrations deviate more significantly from the measured values exceeding the calculated values and with large discrepancies in the first two samples which again questions whether Br behaves conservatively.

6 Dispersion - comparison with continuous push-pull experiments

The Tests 1 and 2 were followed by two more push-pull experiments with injection of CO_2-saturated water spiked with methanol, Kr and Xe with intervening injection of CO_2 and then CO_2-saturated water to drive the CO_2 to residual saturation (Patterson et al., 2016; Serno et al., 2016). The push-pull experiments differed from Tests 1 and 2 in that the ratio of volume of water produced to that injected was larger (~ 1.5 versus 0.6) and the water production was continuous without the ~ 10 day pauses of Tests 1 and 2 (Fig. 1). The behaviour of the methanol tracer in these experiments (Fig. 9) matches the
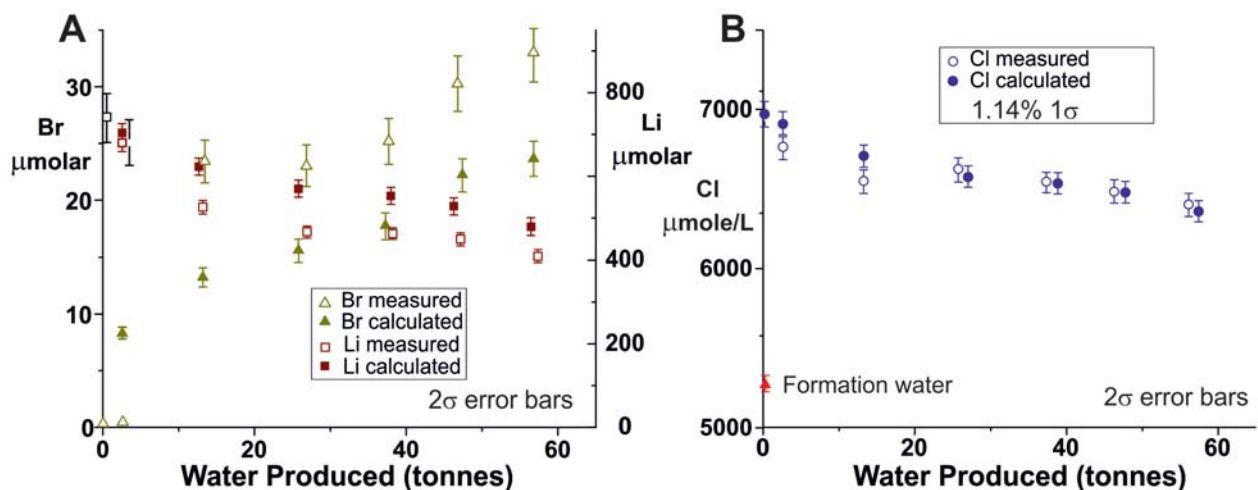
Fig. 8. Comparison of measured Br, Li and Cl concentrations and those calculated from proportions of Test 1 injection, Test 2 injection and formation waters given by Sr systematics. Uncertainties 1σ calculated by a Monte Carlo routine propagating 1σ uncertainties of 5×10^{-6} on Sr-isotope ratios, 3.2% on Sr, 8% on Br, 3.0% on Li and 1.1% on Cl concentrations based on duplicates of Test 2 water samples.
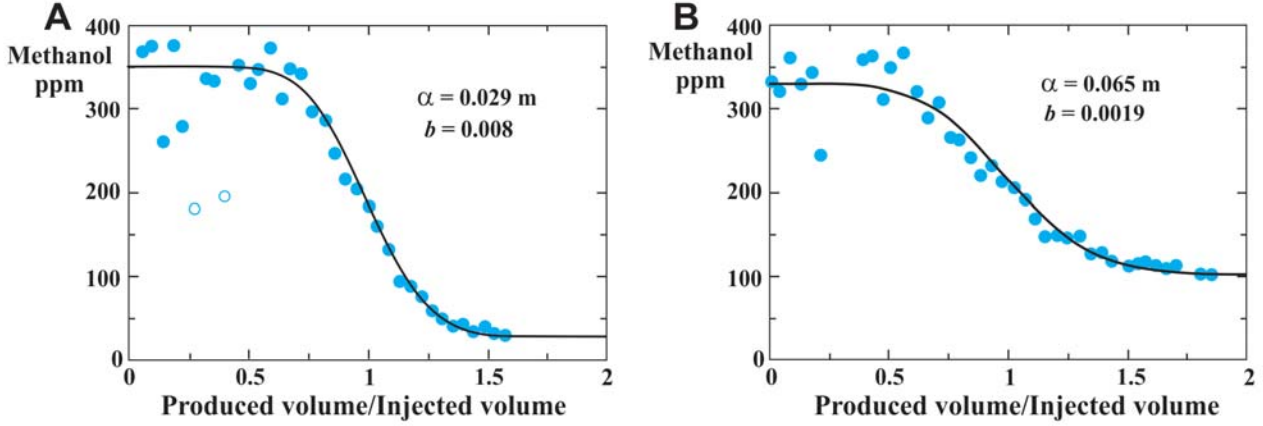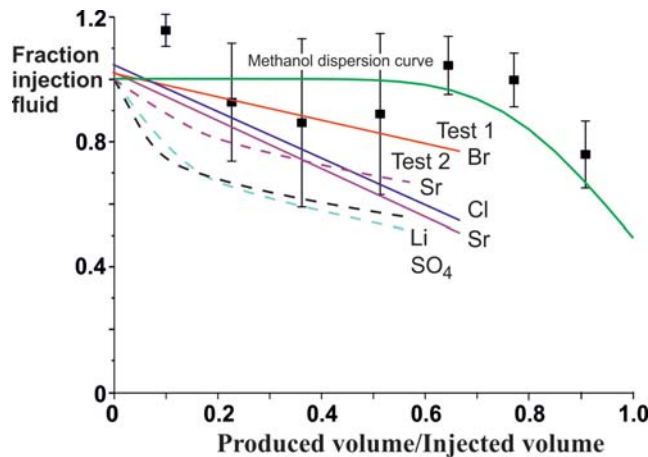
Fig. 9. Dispersion of methanol spike in two push-pull experiments run before (Fig. 9A) and after (Fig. 9B) CO_2 was injected into the reservoir and reduced to residual saturation. Curves are best fits to equation 10 where α is the dispersion distance (c.f. Patterson et al., 2016; Serno et al., 2016). Open symbols excluded from fit.

dispersions expected from field injection experiments over several metres length scales (e.g. Neuman, 1990) with the concentrations fit to the complimentary error function expression of Gelhar and Collins, (1971) for a recharge-pumping cycle in a confined aquifer as

$$C = \frac{(C_{inj} - C_f)}{2} . erfc \left[\frac{x-1}{\left[\frac{16b}{3} \left(2 - \sqrt{|1-x|}(1-x) \right) \right]^{0.5}} \right] \qquad 10$$

where x is the ratio of produced water/injected water and b a constant which relates to the radial dispersivity b, as $b = \alpha.L$ where L is the characteristic fluid penetration distance (~3.7 m). The dispersivity, α, increases from~ 0.029 m prior to CO_2 injection (Fig. 9A) to ~ 0.065 m in the reservoir with CO_2 at residual saturation (Fig. 9B) reflecting the reduced accessible porosity available in the latter.

The dilution of all the tracers in Tests 1 and 2 initiates significantly earlier than implied by the best fit to the methanol injection experiments (Fig. 10). Further Test 2 exhibits faster initial dilution than Test 1. The injection (between 120 and 200 t/day) and production (~ 50 t/day) rates of all the experiments are broadly similar precluding fluid velocity differences significantly impacting dispersion. However the methanol concentrations in the first produced waters tend to decrease while produced water/injected water < 0.5 although not as fast as the tracers in Tests 1 and 2 and the methanol concentrations exhibit significantly more scatter than the Test 1 and 2 tracers. A major difference is that in the Test 1 and Test 2 experiments there were ~ 10 day pauses between the phases of water pro-

Fig. 10. Schematic dilution curves for the key tracers in Tests 1 (solid lines) and 2 (broken lines) (the data are shown on Figs. 3 and 5). These are compared to the best fit dispersion curve predicted from the methanol-spiked injection prior to CO_2 injection (Fig. 9A) which implies methanol concentration in the injected fluid of 343 ppm. Squares and 1σ error bars are three-point averages of methanol concentrations.
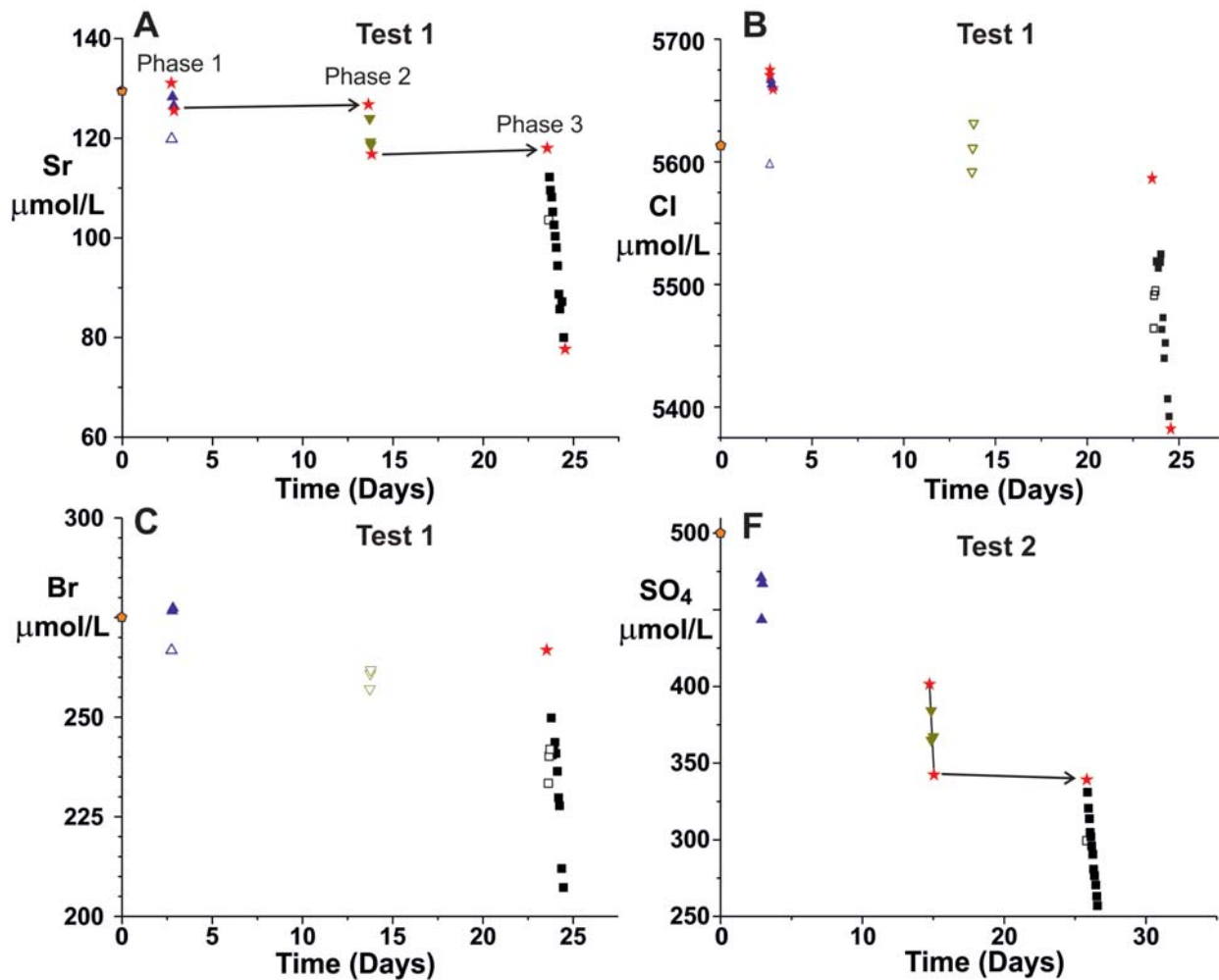
Fig. 11. Sr, Cl and Br concentration in produced waters (Test 1) and SO_4 concentrations (Test 2) versus time. Open symbols show samples excluded from fits (generally the initial samples which have lower concentrations). Red stars show sample composition inferred from each regression extrapolated to times production was initiated and terminated in the respective phase. Solid horizontal arrows emphasise consistency of composition between the estimated compositions of the final sample of production phases 1 and 2 and the initial sample of the subsequent phase for Sr in Test 1 and SO_4 between phase 2 and 3 in Test 2. Cl and Br concentrations both increase or scatter in phase 2 of Test 1 and realistic estimates of the initial and final compositions are not possible.

duction. One possibility is that mixing takes place during the pauses in production either by diffusion between the fluid masses or by small residual flows of the fluids caused by adjustment of pressure or density differences after the pumping pauses. This can be tested by looking for changes in fluid composition between the production phases. The low concentrations in the initial samples in each phase of production have been discussed above noting that these were taken after only between 2.5 and 5 tonnes of production. The atypically low concentrations may be attributed to mixing with ~ 0.4 tonne of fluid potentially sourced from the borehole and borehole damage zone although this may include extraction of poorly mixed fluids in the reservoir near the borehole. However it is possible to extrapolate the composition trends of the subsequent samples from the phase 2 and 3 production episodes to infer the initial fluid composition at the start of the phase 2 and 3 production with that at the end of phase 1 and phase 2 for Sr in Test 1 and between the end on phase 2 and start of phase 3 for SO_4 in Test 2 (Fig. 11). For these 'well behaved' tracers there is no evidence of significant dilution between the pumping phases. What is curious is the different behaviours of the tracers during the initial pumping. For example in Test 1, phase 3, only the Sr concentration of the initial sample lies below the linear trend of the
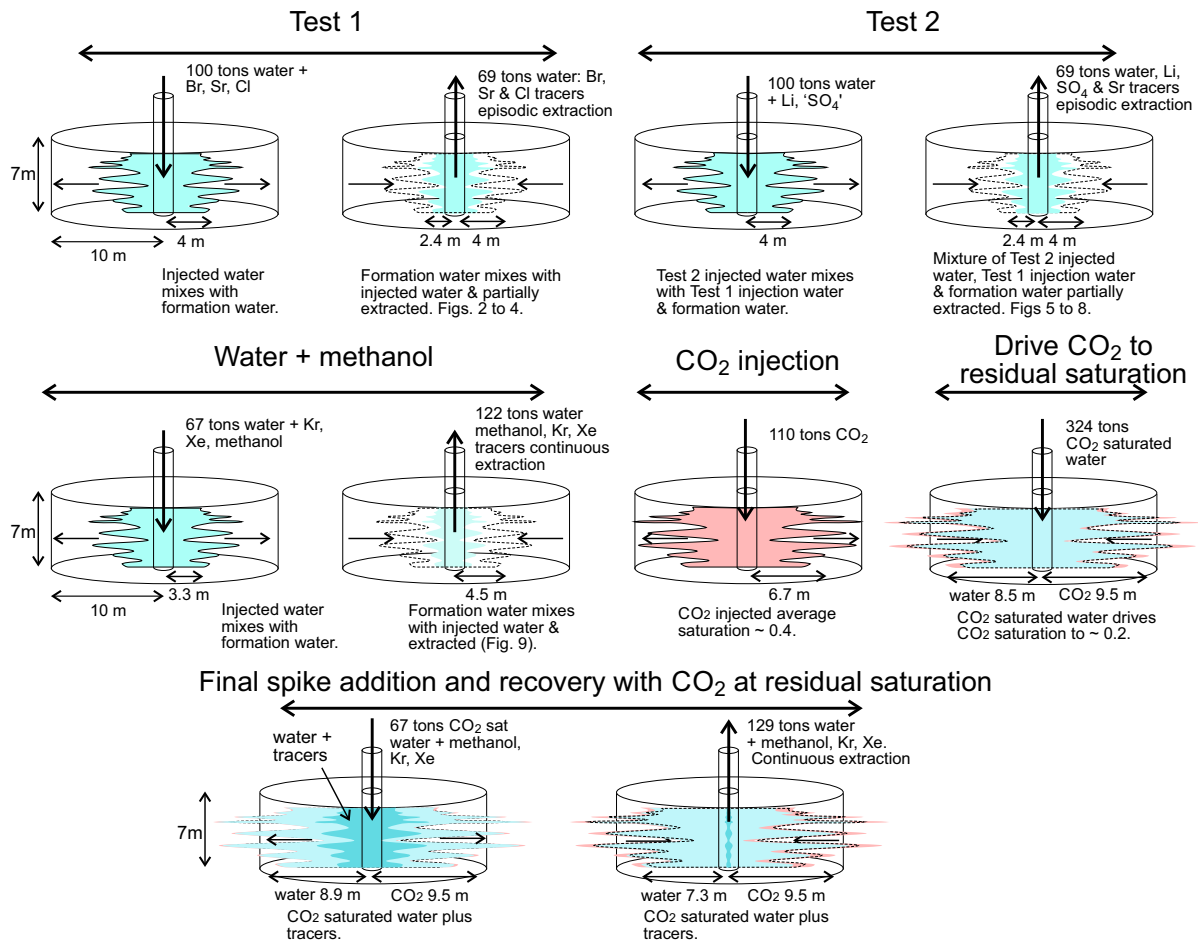
Fig. 12. Schematic illustration of the injection/extraction phases during the 2B extension experiments. Blue shading indicates extent of water injections and red CO_2. Note that there is only partial extraction of water with injected tracers in Tests 1 and 2. Tracer measurements show impact of mixing which increases the further fluids travel from the well and then are extracted towards the well. The diagram of CO_2 distribution does not attempt to show the movement of the CO_2 plume towards the top of the permeable interval or the continued migration of the plume after injection documented by Ennis-King et al, (2017).

remaining samples whereas the Br and Cl concentrations of the first three samples are low compared to a regression through the remaining samples.

The scatter to low values in the methanol samples at produced water to injected water ratios of < 0.6 (Fig. 9A) suggests that mixing near the well bore is incomplete and on extraction the poorly mixed formation waters are extracted preferentially as suggested by Pickens and Grisak (1981). A similar explanation was suggested by Haese et al., (2013) for early breakthrough of CO_2-saturated waters in a previous CO_2 dissolution experiment at Otway. The more rapid dilution of the samples from the spaced pumping phases in Tests 1 and 2 must reflect some consequence of the pauses in production. Possible causes might include 1) diffusive exchange increasing away from the borehole if more distal fluids occupy thinner horizons and contact more formation water, 2) residual flows of formation waters after pumping ceases (but why should the distal fluids exhibit more dilution?) or 3) the injection opening up cracks which close over time favouring extraction from lower permeability horizons proximal to the well bore. Alternatively fluids may be diluted by extraction from overlying or underlying formations through the damage zone around the borehole although this would be expected to occur throughout the production phases and in the subsequent experiments.

A further observation is that the shape of the dilution curves in Test 2 shows more rapid early dilution than Test 1 (Fig. 10) implying some change in the porosity and permeability structure of the reser-

voir with Test 2. Since permeability is a very sensitive function of porosity, minor dissolution of carbonate, sulphide or Fe-oxyhydroxide phases might change the permeability of the near well-bore region sufficiently to impact fluid mixing.

Figure 12 illustrates the history of injection and extraction schematically and it is important to remember that each injection/extraction experiment is superimposed on the fluid state left by the previous experiments and that the 2014 Stage 2B extension tests modelled here were preceeded by a comparable series, the 2B experiments in 2011.

7   Conclusions.

The additional analyses of Sr-isotopic ratios demonstrates the utility of isotopic measurements to confirm modelling of processes based on concentration data alone. In general Sr and Cl (Test 1) and Sr, Li and SO_4 in Test 2 indicate comparable amounts of mixing of injection waters with formation waters in the push-pull experiments. There appear to be a significant differences in the tracer recovery curves between the Test 1 and 2 push-pull experiments, with significant pauses in production, and the continuous injection-production experiments with methanol as a tracer. Confirmation of these will require the push-pull experiments with significant pauses in production to be run to higher produced water to injected water ratios to sample the full dispersion curves and preferably use chemically comparable tracers in both paused and continuous production experiments. Also the pumping phases in the paused push-pull experiments should extract ~ 50 tons (following 100 ton injections) so that any initial variability due to well bore mixing is eliminated. A U-tube sample from the wellbore immediately before pumping initiates would sample the wellbore fluid to confirm the cause of the low concentrations in early-produced samples.

The ultimate objectives of such experiments should be to establish if the dispersion curves can be used as measures of formation heterogeneity and to determine the extent that the dilution of injection fluids is driven by mixing of fluids by flow processes versus diffusion of tracers between fluid flow paths. Achieving this objective will require assessment of the various tracers to establish which behave conservatively and a proper understanding of the causes of the variations in mixing as fluids are extracted from the formations.

Acknowledgements

Declarations of Interest: None

References

Benson, S.M., Bickle, M., Boon, M., Cook, P.J., Haese, R., Kurtev, K., Matthai, S., Neufeld, J., Watson, M., Winkelman, G.,. 2018. The GeoCquest Project: Quantifying the impact of heterogeneity on CO_2 migration and trapping in saline aquifers, 14th International Conference on Greenhouse Gas Control Technologies, 21-26 October 2018, GHGT-14, Melbourne, 9 p. https://ssrn.com/abstract=3366097.

Black, J.R., Vu, H.P., Haese, R.R., 2017. Aqueous phase tracers for monitoring fluid mixing in geological reservoirs: Results from two field studies. International Journal of Greenhouse Gas Control, 67: 103-110.

Dance, T., Paterson, L., 2016. Observations of carbon dioxide saturation distribution and residual trapping using core analysis and repeat pulsed-neutron logging at the CO2CRC Otway site. International Journal of Greenhouse Gas Control, 47: 210-220.

Ennis-King, J., LaForce, T., Paterson, L., Black, J. R., Vu, H. P., Haese, R. R., Serno, S., Gilfillan, S., Johnson, G., Freifeld, B., Singh, R., 2017. Stepping into the same river twice: field evidence for the repeatability of a CO_2 injection test. Energy Procedia, 114: 2760 - 2771.

Gelhar, L.W., Collins, M.A., 1971. General analysis of longitudinal dispersion in nonuniform flow. Water Resources Research, 7(6): 1511-1521.

Haese, R., LaForce, T., Boreham, C., Ennis-King, J., Freifeld, B. M., Paterson, L., Schact, U., 2013. Determining residual CO_2 saturation through a dissolution test - results from the CO2CRC Otway project. Energy procedia, 37: 5379-5386.

Haese, R.R., Black, J.R., Vu, H.P., 2016. The impact of impurities (SO_2, NO_x, O_2) on fluid-rock reactions and water quality in a CO2 storage reservoir - Results from the Stage 2B extension phase 1. CO2CRC publication number RPT16-5501, Melbourne.

Hovorka, S., Benson, S., Doughty, C., Freifeld, B., Sakurai, S., Daley, T., Kharaka, Y., Holtz, M., Trautz, R., Nance, H., 2006. Measuring permanence of CO_2 storage in saline formations: the Frio experiment. Environmental Geosciences, 13: 105.

Hovorka, S. D., Meckel, T. A., Trevino, R. H., Lu, J., Nicot, J.-P., Choi, J.-W., Freeman, D., Cook, P., Daley, T. M., Ajo-Franklin, J. B., Freifeild, B. M., Doughty, C., Carrigan, C. R., La Brecque, D., Kharaka, Y. J., Thordsen, J. J., Phelps, T. J., Yang, C., Romanak, K. D., Zhang, T., Holt, R. M., Lindler, J. S., Butsch, R. J., 2011. Monitoring a large volume CO_2 injection: Year two results from SECARB project at Denbury's Cranfield, Mississippi, USA. Energy Procedia, 4: 3478-3485.

Kampman, N., Busch, A., Bertier, P., Snippe, J., Hangx, S., Pipich, V., Di, Z., Rother, G., Harrington, J. F., Evans, J. P., Maskell, A., Chapman, H. J., Bickle, M. J., 2016. Observational evidence confirms modelling of the long-term integrity of CO_2-reservoir caprocks. Nature Communications, 7: 10.

Kirste, D., Haese, R., Boreham, C., Schacht, U., 2014. Evolution of formation water chemistry and geochemical modelling of the CO2CRC Otway Site residual gas saturation test. Energy Procedia, 63: 2894-2902.

LaForce, T., Freifeld, B.M., Ennis-King, J., Boreham, C., Paterson, L., 2014. Residual CO_2 saturation estimate using noble gas tracers in a single-well field test: The CO2CRC Otway project. International Journal of Greenhouse Gas Control, 26: 9-21.

Myers, M., Stalker, L., La Force, T., Pejcic, B., Dyt, C., Ho, K.-B., Ennis-King, J., 2015. Field measurement of residual carbon dioxide saturation using reactive ester tracers. Chemical Geology, 399: 20-29.

Neuman, S.P., 1990. Universal Scaling of Hydraulic Conductivities and Dispersivities in Geologic Media. Water resources research, 26: 1749-1758.

Paterson, L., Boreham, C., Bunch, M., Dance, T., Ennis-King, J., Freifeld, B., Haese, R., Jenkins, C., Raab, M., Singh, R., Stalker, L., 2014. Otway Stage 2B residual saturation and dissolution test. In: Cook, P.J. (Ed.), Geologically Storing Carbon: Learning from the Otway Project Experience. CSIRO Publishing, Melbourne, Australia, pp. 329-360.

Paterson, L., Ennis-King, J., LaForce, T., Gillfillan, S., Serno, S., Johnson, G., Boreham, C., Dance, T., Freifeild, B., Singh, R., 2016. CO2CRC Otway Stage 2B Extension Phase 2. CO2CRC report RPT16-5429.

Pickens, J.F., Grisak, G.E., 1981. Scale-dependent dispersion in a stratified granular aquifer. Water Resources Research, 17(4): 1191-1211.

Serno, S., Johnson, G., LaForce, T. C., Ennis-King, J., Haese, R. R., Boreham, C. J., Paterson, L., Freifeld, B. M., Cook, P. J., Dirk Kirste, D., Haszeldine, R. S., Gilfillan, S. M. V., 2016. Using oxygen isotopes to quantitatively assess residual CO_2 saturation during the CO2CRC Otway Stage 2B Extension residual saturation test. International Journal of Greenhouse Gas Control, 52: 73-83.

Stalker, L., Boreham, C., Underschultz, J., Freifeld, B., Perkins, E., Schacht, U., Sharma, S., 2015. Application of tracers to measure, monitor and verify breakthrough of sequestered CO_2 at the CO2CRC Otway Project, Victoria, Australia. Chemical Geology, 399: 2-19.

Vu, H.P., Black, J.R., Haese, R.R., 2017. Changes in formation water composition during water storage at surface and post re-injection. Energy Procedia, 114: 5732-5741.

Vu, H.P., Black, J.R., Haese, R.R., 2018. The geochemical effects of O_2 and SO_2 as CO_2 impurities on fluid-rock reactions in a CO_2 storage reservoir. International Journal of Greenhouse Gas Control, 68: 86-98.